

Partial wave contributions to the antikaon potential at finite momentum

Laura Tolós, Angels Ramos, Artur Polls

*Departament d'Estructura i Constituents de la Matèria, Universitat de Barcelona,
Diagonal 647, 08028 Barcelona, Spain*

Thomas T.S. Kuo

*Department of Physics and Astronomy, State University of New York,
Stony Brook, NY 11794, USA*

(October 24, 2018)

Abstract

The momentum dependence of the antikaon optical potential in nuclear matter is obtained from a microscopic and self-consistent calculation using the meson-exchange Jülich $\bar{K}N$ interaction. Two self-consistent schemes are discussed, which would lead to substantially different predictions for the width of \bar{K} nuclear bound states. The effect of higher partial waves of the $\bar{K}N$ interaction, beyond the $L = 0$ component, is studied and found to have moderate but non-negligible effects on the \bar{K} nuclear potential at zero momentum. At momenta as large as 500 MeV/c, relevant in the analysis of heavy-ion collisions, the higher partial waves modify the \bar{K} optical potential by nearly a factor of two.

PACS: 12.38.Lg, 13.75.Jz, 14.40.Ev, 21.30.Fe, 21.65.+f, 25.80.Nv

Keywords: $\bar{K}N$ interaction, Kaon-nucleus potential.

I. INTRODUCTION

Understanding the behavior of matter under extreme conditions of density and temperature, such as those found in neutron stars or in heavy-ion collisions, requires a good knowledge and control on the modification of the properties of hadrons in the nuclear medium. In particular, the in-medium effects on antikaons have received much attention over the last years, especially after the speculation of the possible existence of an antikaon condensed phase [1].

Empirical analysis of kaonic atoms [2] predict a strong attractive K^- -nucleus potential, but, recently, the data have also been shown to be compatible with a potential which is four times less attractive [3]. This last potential was obtained from a microscopic self-consistent calculation [4] using the chiral non-perturbative model of ref. [5] that reproduces the $\bar{K}N$

scattering observables. A recent fine-tuning of this potential [6], was shown to produce a χ^2 as low as that of ref. [2]. These observations imply that the data on kaonic atoms, although giving a strong indication of attraction, do not really constrain the size of the K^- optical potential at nuclear matter saturation density.

The dynamics of the $\bar{K}N$ interaction is particularly rich due to the presence of an isospin 0 resonance, the $\Lambda(1405)$, which lies only 27 MeV below the $\bar{K}N$ threshold. As a result, the isospin averaged $\bar{K}N$ interaction in free space is in fact repulsive. It was soon pointed out, however, that in the medium the Pauli blocking on nucleon states moves the resonance to higher energies and makes the interaction attractive [7–9]. This particular (resonant-like) energy dependence of the $\bar{K}N$ interaction at subthreshold energies requires an especially careful treatment of all in-medium effects. In fact, when the attraction felt by the antikaon is self-consistently incorporated in the calculation [10] it compensates partly the effects induced by Pauli blocking and the Λ resonance gets broader and moves back to lower energies, around its free space location. Moreover, since an extremely important ingredient to generate the Λ resonance is the coupling of the $\bar{K}N$ system to the $\pi\Sigma$ one, the modification of the pion properties was also included in ref. [4], with the result that the resonance width increased further more and the peak shifted upwards to an energy slightly above the free space one.

Heavy-ion collisions can also provide information on the modification of hadronic properties. In particular the enhanced K^-/K^+ ratio measured at GSI [11] can also be understood assuming that the antikaons feel a strong attraction [12–15]. This lowers the threshold for K^- production, hence enhancing the ratio at subthreshold energies. In a recent work [16], it has been shown that the increase on this ratio could also be explained from the in-medium enhanced production of antikaons through Σ hyperons due to the shifting of the $\Lambda(1405)$ resonance to higher energies, a mechanism that was already suggested in ref. [17] to explain the data of K^- absorption at rest on ^{12}C [18,19].

The situation on the antikaon properties in the medium is, at present, far from being clear. Although it is commonly accepted that to explain kaonic atom data and the results on heavy-ion collisions the K^- must feel some attraction, the magnitude of it has not been really determined by the available observations.

One may aim at extracting this information from theoretical models that have been well constrained in free space by the $\bar{K}N$ scattering observables. Due to the special dynamics of the $\bar{K}N$ interaction, these models must treat carefully all medium effects, as well as the energy and momentum dependences of the in-medium $\bar{K}N$ interaction. The momentum dependence of the \bar{K} optical potential is particularly important in the analysis of heavy-ion collisions since antikaons are created at a finite momentum of around 250 – 500 MeV/c.

Intimately connected with the momentum dependence is the role of higher partial waves of the $\bar{K}N$ interaction. For a relative momentum of the $\bar{K}N$ pair as large as that explored in heavy-ion collisions, the importance of the higher partial waves, beyond the commonly considered $L = 0$ component, might become quite relevant.

The purpose of the present work is to study all these effects using the $\bar{K}N$ interaction of the Jülich group [20], which is based on meson-exchange. The Jülich potential predicts the $\Lambda(1405)$ resonance to be a quasibound $\bar{K}N$ state and reproduces satisfactorily the $\bar{K}N$ scattering observables. The matrix elements of this interaction depend on the incident and outgoing three-momenta, as well as on the total invariant center-of-mass energy. A partial wave decomposition is also given in ref. [20], hence allowing the investigation on how the

different partial waves contribute to the \bar{K} optical potential in the nuclear medium.

The paper is organized as follows. In Sect. II we present the formalism to derive the in-medium effective $\bar{K}N$ interaction and the corresponding \bar{K} optical potential. Our results are shown in Sect. III, where particular attention is paid to study the effects of the higher partial waves on the \bar{K} optical potential as obtained with two different self-consistent schemes. Our conclusions are summarized in Sect. IV.

II. IN-MEDIUM $\bar{K}N$ INTERACTION AND \bar{K} OPTICAL POTENTIAL IN NUCLEAR MATTER

In this section we present the formalism to obtain the self-energy or single-particle potential of a \bar{K} meson embedded in infinite symmetric nuclear matter. This self-energy accounts for the interaction of the \bar{K} with the nucleons and its calculation requires the knowledge of the in medium $\bar{K}N$ interaction, which we will describe by a G -matrix. The medium effects incorporated in this G -matrix include the Pauli blocking on the nucleons in the intermediate states as well as the dressing of the \bar{K} and the different baryon lines. We will explore different ways of dressing the intermediate states in solving the G -matrix, which will define the type of self-consistency of the calculation giving rise to the different approaches discussed in this paper.

A. Effective $\bar{K}N$ interaction

The effective $\bar{K}N$ interaction in the nuclear medium or G -matrix is obtained from the bare $\bar{K}N$ interaction derived in the meson exchange framework [20]. As the bare interaction allows for the transition from the $\bar{K}N$ channel to the $\pi\Sigma$ and $\pi\Lambda$ channels, all having strangeness $S = -1$, we are confronted with a coupled channel problem. The resultant meson-baryon (MB) G -matrices can be grouped in a matrix notation, where each box corresponds to one channel. The $\bar{K}N$ channel can have isospin $I = 0$ or $I = 1$. In the first case, it can only couple to the $\pi\Sigma$ channel and the corresponding matrix has the following structure

$$\begin{pmatrix} G_{\bar{K}N \rightarrow \bar{K}N} & G_{\bar{K}N \rightarrow \pi\Sigma} \\ G_{\pi\Sigma \rightarrow \bar{K}N} & G_{\pi\Sigma \rightarrow \pi\Sigma} \end{pmatrix},$$

while for $I = 1$ it can couple to both the $\pi\Sigma$ and $\pi\Lambda$ channels

$$\begin{pmatrix} G_{\bar{K}N \rightarrow \bar{K}N} & G_{\bar{K}N \rightarrow \pi\Sigma} & G_{\bar{K}N \rightarrow \pi\Lambda} \\ G_{\pi\Sigma \rightarrow \bar{K}N} & G_{\pi\Sigma \rightarrow \pi\Sigma} & G_{\pi\Sigma \rightarrow \pi\Lambda} \\ G_{\pi\Lambda \rightarrow \bar{K}N} & G_{\pi\Lambda \rightarrow \pi\Sigma} & G_{\pi\Lambda \rightarrow \pi\Lambda} \end{pmatrix}.$$

Keeping this structure in mind, the G -matrix is formally given by

$$\begin{aligned} \langle M_1 B_1 | G(\Omega) | M_2 B_2 \rangle &= \langle M_1 B_1 | V(\sqrt{s}) | M_2 B_2 \rangle \\ &+ \sum_{M_3 B_3} \langle M_1 B_1 | V(\sqrt{s}) | M_3 B_3 \rangle \frac{Q_{M_3 B_3}}{\Omega - E_{M_3} - E_{B_3} + i\eta} \langle M_3 B_3 | G(\Omega) | M_2 B_2 \rangle \quad (1) \end{aligned}$$

In Eq. (1), M_i and B_i represent the possible mesons (\bar{K} , π) and baryons (N , Λ , Σ), respectively, and their corresponding quantum numbers such as spin, isospin, strangeness, and linear momentum. The function Q_{M_3, B_3} stands for the Pauli operator which allows only intermediate nucleon states compatible with the Pauli principle. The energy variable Ω is the so called starting energy that we will always take as a real quantity, while \sqrt{s} is the invariant center-of-mass energy which enters into the definition of the bare potential [20], i.e. $\sqrt{s} = \sqrt{\Omega^2 - P^2}$, where (Ω, \vec{P}) is the total meson-baryon fourmomentum in a frame in which nuclear matter is at rest.

The former equation for the G -matrix has to be considered together with a prescription for the single-particle energies of all the mesons and baryons participating in the reaction and in the intermediate states. These energies can be written as

$$E_{M_i(B_i)}(k) = \sqrt{k^2 + m_{M_i(B_i)}^2} + U_{M_i(B_i)}(k, E_{M_i(B_i)}^{qp}), \quad (2)$$

where $U_{M_i(B_i)}$ is the single-particle potential of each meson (baryon) calculated at the real quasi-particle energy $E_{M_i(B_i)}^{qp}$, obtained by solving the following equation

$$E_{M_i(B_i)}^{qp}(k) = \sqrt{k^2 + m_{M_i(B_i)}^2} + \text{Re} U_{M_i(B_i)}(k, E_{M_i(B_i)}^{qp}). \quad (3)$$

In the present paper we have considered the single-particle potential for the \bar{K} meson and all baryons. While for the Λ and Σ hyperons we use the simplified form

$$U_{\Lambda, \Sigma} = -30 \frac{\rho}{\rho_0}, \quad (4)$$

where ρ_0 is the saturation nuclear matter density, for nucleons we take the density dependent parametrization [21]

$$U_N(\rho, k) = \alpha(\rho) + \frac{\beta(\rho)}{1 + \left[\frac{k}{\gamma(\rho)} \right]^2}, \quad (5)$$

that was fitted to the single-particle potentials obtained from variational calculations using realistic NN interactions. The density-dependent real parameters $\alpha(\rho)$, $\beta(\rho)$ and $\gamma(\rho)$ are given in Table I of ref. [21]. The nucleon potential at $\rho = \rho_0$ amounts to -70 MeV.

In the Brueckner-Hartree-Fock approach, the \bar{K} self-energy is schematically given by

$$U_{\bar{K}}(k, E_{\bar{K}}^{qp}) = \sum_{N \leq F} \langle \bar{K}N | G_{\bar{K}N \rightarrow \bar{K}N}(\Omega = E_N^{qp} + E_{\bar{K}}^{qp}) | \bar{K}N \rangle, \quad (6)$$

where the summation over nucleon states is limited by the nucleon Fermi momentum.

At the required \bar{K} energies, the G -matrix in the above equation becomes complex due to the possibility of $\bar{K}N$ decaying into the $\pi\Sigma$, $\pi\Lambda$ channels. As a consequence, the potential $U_{\bar{K}}$ is also a complex quantity. The explicit calculation of $U_{\bar{K}}$ will be discussed in the next subsection.

The influence of the medium on the G -matrix is studied by considering different approaches to the self-consistent single-particle energy used for the \bar{K} meson in Eq. (1). We have taken two prescriptions: a) the real quasi-particle energy defined in Eq. (3) and b) the

complex $E_{\bar{K}}$ defined in Eq. (2) which also contains the imaginary part of $U_{\bar{K}}$ calculated at $E_{\bar{K}}^{qp}$.

We solve the G -matrix equation by doing first a partial wave decomposition. Using the quantum numbers of the relative and center-of-mass motion, the G -matrix equation in this basis reads

$$\begin{aligned} \langle (M_1 B_1); k'' | G^{LJI}(P, \Omega) | (M_2 B_2); k \rangle &= \langle (M_1 B_1); k'' | V^{LJI}(\sqrt{s}) | (M_2 B_2); k \rangle \\ &+ \sum_{M_3 B_3} \int k'^2 dk' \langle (M_1 B_1); k'' | V^{LJI}(\sqrt{s}) | (M_3 B_3); k' \rangle \\ &\times \frac{\bar{Q}_{M_3 B_3}(k', P)}{\Omega - \sqrt{M_{B_3}^2 + \widetilde{k}_{B_3}^2} - \sqrt{M_{M_3}^2 + \widetilde{k}_{M_3}^2} - U_{B_3}(\widetilde{k}_{B_3}^2) - U_{M_3}(\widetilde{k}_{M_3}^2) + i\eta} \\ &\times \langle (M_3 B_3); k' | G^{LJI}(P, \Omega) | (M_2 B_2); k \rangle, \end{aligned} \quad (7)$$

where the variables k, k', k'' and L denote relative linear momenta and orbital momentum, respectively, while P is the linear center-of-mass momentum. The functions \widetilde{k}_B^2 and \widetilde{k}_M^2 are, respectively, the square of the momentum of the baryon and that of the meson in the intermediate states, averaged over the angle between the total momentum \vec{P} and the relative momentum \vec{k}' (see the definitions in appendix A)

$$\widetilde{k}_B^2(k', P) = k'^2 + \left(\frac{M_B}{M_M + M_B} \right)^2 P^2 \quad (8)$$

$$\widetilde{k}_M^2(k', P) = k'^2 + \left(\frac{M_M}{M_M + M_B} \right)^2 P^2. \quad (9)$$

The angle average of the Pauli operator, $\bar{Q}_{M_3 B_3}(k', P)$, is shown explicitly in appendix A and differs from unity only in the case of the $\bar{K}N$ channel. The total angular momentum and isospin are denoted by J and I , respectively. For each J , two values of orbital angular momentum, $L = J + 1/2$ and $L = J - 1/2$, are allowed. However, due to parity conservation, the interaction can not mix these two states and, as a consequence, the orbital angular momentum is also a conserved quantity.

B. \bar{K} single-particle energy in Brueckner-Hartree-Fock approximation

By using the partial wave decomposition of the G -matrix, the Brueckner-Hartree-Fock approximation to the single-particle potential of a \bar{K} meson embedded in a Fermi sea of nucleons [Eq. (6)] becomes

$$\begin{aligned} U_{\bar{K}}(k_{\bar{K}}, \omega = E_{\bar{K}}^{qp}(k_{\bar{K}})) &= \frac{1}{2} \sum_{L, J, I} (2J + 1)(2I + 1)(1 + \xi)^3 \int_0^{k_{max}} k^2 dk f(k, k_{\bar{K}}) \\ &\times \langle (\bar{K}N); k | G^{LJI}(\overline{P^2}, E_{\bar{K}}^{qp}(k_{\bar{K}}) + E_N^{qp}(\overline{k_N^2})) | (\bar{K}N); k \rangle, \end{aligned} \quad (10)$$

where $\overline{P^2}$ and $\overline{k_N^2}$ are the square of the center-of-mass momentum and nucleon momentum, respectively, averaged over the angle between the external \bar{K} momentum in the lab system, $\vec{k}_{\bar{K}}$, and the $\bar{K}N$ relative momentum, \vec{k} , used as integration variable in Eq. (10) (see

appendix B for details). These angle averages eliminate the angular dependence of the G -matrix and allow to perform the angular integration in Eq. (10) analitically, giving rise to the weight function, $f(k, k_{\bar{K}})$,

$$f(k, k_{\bar{K}}) = \begin{cases} 1 & \text{for } k \leq \frac{k_F - \xi k_{\bar{K}}}{1 + \xi}, \\ 0 & \text{for } |\xi k_{\bar{K}} - (1 + \xi)k| > k_F, \\ \frac{k_F^2 - [\xi k_{\bar{K}} - (1 + \xi)k]^2}{4\xi(1 + \xi)k_{\bar{K}}k} & \text{otherwise,} \end{cases} \quad (11)$$

where $\xi = \frac{M_N}{M_{\bar{K}}}$ and k_F is the Fermi momentum. The magnitude of the relative momentum k is constrained by

$$k_{max} = \frac{k_F + \xi k_{\bar{K}}}{1 + \xi}. \quad (12)$$

After self-consistency for the on-shell value $U_{\bar{K}}(k_{\bar{K}}, E_{\bar{K}}^{qp})$ is achieved, one can obtain the complete energy dependence of the self-energy, $U_{\bar{K}}(k_{\bar{K}}, \omega)$, which can be used to determine the \bar{K} single-particle propagator in the medium,

$$D_{\bar{K}}(k_{\bar{K}}, \omega) = \frac{1}{\omega^2 - k_{\bar{K}}^2 - m_{\bar{K}}^2 - 2m_{\bar{K}}U_{\bar{K}}(k_{\bar{K}}, \omega)}, \quad (13)$$

and the corresponding spectral density

$$S_{\bar{K}}(k_{\bar{K}}, \omega) = -\frac{1}{\pi} \text{Im} D_{\bar{K}}(k_{\bar{K}}, \omega). \quad (14)$$

III. RESULTS

We start this section by showing explicitly the most characteristic medium modification of the $\bar{K}N$ amplitude, which is obtained when the Pauli blocking on the intermediate nucleons is incorporated. The real and imaginary parts of the resulting in-medium $\bar{K}N$ amplitudes for a total momentum $|\vec{k}_{\bar{K}} + \vec{k}_N| = \vec{0}$ are shown in Fig. 1 as functions of the invariant center-of-mass energy, for three different densities: $\rho = 0$ (dotted lines), $\rho = \rho_0/2$ (dot-dashed lines), and $\rho = \rho_0$ (solid lines), with $\rho_0 = 0.17 \text{ fm}^{-3}$ being the saturation density of nuclear matter. We clearly see, as noticed already by all earlier microscopic calculations, the repulsive effect on the resonance produced by having moved the threshold of intermediate allowed $\bar{K}N$ states to higher energies, as a result of Pauli blocking acting on the nucleon.

Clearly, this shift of the resonance changes the $\bar{K}N$ interaction at threshold (~ 1432 MeV) from being repulsive in free space to being attractive in the medium. Since this effect is intimately connected with the strong energy dependence of the $\bar{K}N$ interaction, important changes can be expected from a self-consistent incorporation of the \bar{K} properties on the $\bar{K}N$ G -matrix, as already noted by Lutz [10] and confirmed in ref. [4].

This type of self-consistent calculations are also common in Brueckner-Hartree-Fock studies of the NN interaction, where it is costumary to take the nucleon single-particle energies as

real quantities. This amounts to disregard the imaginary part of the in medium NN amplitude in the calculation of the single-particle energy for nucleons above the Fermi momentum. We have attempted a similar type of approximate scheme for the \bar{K} meson, although in this case the $\bar{K}N$ amplitude is already complex at threshold due to the $\pi\Lambda$, $\pi\Sigma$ channels. In this simplified self-consistent scheme, only the real part of the \bar{K} potential is retained in the solution of the G -matrix, i.e. the \bar{K} energy appearing in Eq. (1) is taken to be the real quasi-particle energy of Eq. (3).

Once self-consistency is achieved, we calculate both real and imaginary parts of the \bar{K} potential, which are displayed in Fig. 2 as functions of the antikaon momentum, for normal nuclear matter density $\rho = \rho_0$. We explicitly show the separate contribution of the various partial waves of the $\bar{K}N$ interaction. At zero momentum the real part of the \bar{K} potential is about -100 MeV and the partial waves higher than the $L = 0$ component give a negligible contribution. Both the real and imaginary parts of the potential show some structure between 200 MeV/c and 400 MeV/c. This is connected to the behavior of the in-medium $\bar{K}N$ amplitude which, in this simplified self-consistent scheme, still retains the resonant-like shape at $\rho = \rho_0$. We observe that the high partial waves start being non-negligible for momenta larger than 200 MeV/c. It is interesting to focus our attention on the imaginary part of the \bar{K} potential which at low momentum is rather small. This is due to the suppressed coupling to intermediate $\pi\Sigma$ states as a result of the strong attraction felt by the antikaon combined with the attraction of around -70 MeV felt by the nucleon. The in-medium $\bar{K}N$ system then explores energies below those available for $\pi\Sigma$ excitations and the antikaon width becomes extremely small. In this low momentum region the imaginary part of the \bar{K} potential is essentially due to the coupling to $\pi\Lambda$ states in the relatively weak $I = 1$ channel. As seen in the figure, for the $\pi\Sigma$ channel to start giving a contribution to the imaginary part, it is necessary to provide the \bar{K} with a finite momentum (around 200 MeV/c), such that the condition $E_{\bar{K}}^{qp} + E_N^{qp} > m_\pi + m_\Sigma + U_\Sigma \simeq 1300$ MeV can be fulfilled.

The substantial attraction obtained for the \bar{K} optical potential combined with the extremely small imaginary component of the \bar{K} optical potential might induce to think that the chances of producing very narrow, hence observable, deeply bound \bar{K} -nucleus states are quite high. If these results were confirmed by more sophisticated treatments of the in-medium effects, an experimental search for these states should be indeed encouraged. However, as we will show in the following, the use of a more realistic self-consistent scheme wears this finding off.

Our second method consists of determining the complete complex \bar{K} single-particle energy given in Eq. (2) self-consistently. That means that the dressing of the \bar{K} in the intermediate states of the G -matrix equation is taken into account through a complex but energy-independent self-energy. This gives rise to the so-called “quasi-particle” spectral density, which has the energy dependence of a Lorentzian distribution. Although this is an approximation with respect to the more sophisticated attempts made in Refs. [4,10], where the full energy dependence of the \bar{K} self-energy is self-consistently determined, it is sufficiently good for the studies we are carrying out in the present work. Moreover, at the end of the self-consistent scheme, we evaluate the spectral density of the \bar{K} keeping the complete momentum and energy dependence of the \bar{K} self-energy.

We first show, in Fig. 3, the effect of dressing the antikaon with a complex self-energy on the in medium $\bar{K}N$ amplitude. Comparing with the results shown in Fig. 1, we observe

that the resonance peak stays now pretty close or even lower than its free space location. As mentioned above, this is due to the attraction felt by the \bar{K} that compensates the repulsive effect induced by Pauli blocking on the nucleon. Secondly, both real and imaginary parts of the $\bar{K}N$ amplitude become much smoother, as a result of the \bar{K} strength being spread out over energies. The resonance gets wider and dilutes much earlier with increasing density. We note that these effects are in total agreement with those obtained with the self-consistent approaches of refs. [4,10].

Our results for the antikaon potential at $\rho = \rho_0$ obtained with this complete self-consistent scheme are shown in Fig. 4. The real part of the \bar{K} potential at zero momentum increases to -87 MeV. It is worth noticing that the new scheme has produced a drastically different imaginary part. The small value of -3 MeV at zero momentum obtained using the simplified scheme turns out to be now around -25 MeV, hence making the observation of bound \bar{K} nuclear states more difficult. This is a consequence of the fact that the in-medium $\bar{K}N$ amplitude becomes smoother and wider when the \bar{K} energies are complex. Since the \bar{K} spectral density develops a width and, in turn, the \bar{K} feels a reduced attraction, the $\bar{K}N$ states can couple more easily to the $\pi\Sigma$ states than in the previous self-consistent scheme. From these results one must conclude that any approach claiming for narrow bound \bar{K} nuclear states must be looked at with caution, because the self-consistent scheme affects enormously the predicted \bar{K} properties in the medium.

The effect of including the higher partial waves of the $\bar{K}N$ interaction is also seen in Fig. 4. We observe that at zero \bar{K} momentum there is already some contribution of partial waves higher than $L = 0$ due to the fact that the \bar{K} meson interacts with nucleons that occupy states up to the Fermi momentum, giving rise to finite $\bar{K}N$ relative momenta of up to around 90 MeV/c. Clearly, the effect of the higher partial waves increases with increasing \bar{K} momentum, flattening out the real part of the optical potential and producing more structure to the imaginary part. At a \bar{K} momentum around 500 MeV/c, the inclusion of higher partial waves makes the real part more attractive, from -28 MeV to -52 MeV, and practically doubles the size of the imaginary part.

In Fig. 5 we represent the real and the imaginary part of $U_{\bar{K}}$ for different densities, obtained with the scheme that considers the complex potential for the antikaon. As we increase the density we obtain a more attractive potential due to two facts. On one hand, as discussed previously, the interaction is more attractive at higher densities. On the other hand, the \bar{K} feels the interaction of many more nucleons. The momentum dependence is moderate for the real part. In contrast, the imaginary part for densities around the saturation density and beyond shows more structure. This momentum dependence is smoother than that obtained in ref. [15] from a phenomenological model using the information of the vacuum $\bar{K}N$ amplitudes, where the antikaon optical potential at normal nuclear matter density ρ_0 increases from -140 MeV at zero momentum to around -50 MeV at high momenta.

Starting from the self-consistent \bar{K} optical potential shown in Fig. 3 and reproduced by the solid line in Fig. 5, we perform two different tests in order to check some of the approximations used in the literature. First, we compute the optical potential neglecting the nucleon recoil corrections, as done in ref. [16]. This amounts to calculate the \bar{K} potential at momentum $k_{\bar{K}}$ from a $G\rho$ type expression, with G being the in-medium $\bar{K}N$ interaction between a \bar{K} of momentum $k_{\bar{K}}$ and a nucleon of zero momentum. The results are displayed by the dashed lines in Fig. 5. While the real part is barely affected by this

simplified approximation, the imaginary part shows some non-negligible differences at low momenta. Secondly, we have neglected, in addition, the nucleon single-particle potential, which has been claimed to be unimportant in ref. [16]. Note that in this later reference a small imaginary part of around 10 MeV for the nucleon optical potential is used, but the real part is set to zero. The results are shown by the dotted line. The differences with the dashed line are quite appreciable at low momenta, both for the real and imaginary parts of the \bar{K} optical potential.

Finally, once self-consistence is reached, we calculate the full energy dependence of the \bar{K} self-energy which defines the in-medium \bar{K} single-particle propagator and its spectral density through Eqs. (13) and (14). The spectral density at zero momentum is shown in Fig. 7 for several densities. As density increases the peak of the \bar{K} pole moves towards lower energies since the \bar{K} optical potential becomes more attractive. The in medium $\Lambda(1405)$ resonance gets wider and, although not signaled by any clear peak in the figure, its presence can be indirectly noticed from examining the \bar{K} spectral density on the right hand side of the quasiparticle peak, which falls off more slowly than that on the left hand side. We also notice some structure of the spectral function to the left of the quasiparticle peak at energies of the \bar{K} of around 320 – 360 MeV, the origin of which can be traced back to a pole of the free $\bar{K}N$ amplitude obtained with the Jülich interaction in the $L = 1, I = 1$ channel at an energy $\sqrt{s} = 1230$ MeV, about 200 MeV below the $\bar{K}N$ threshold. This pole comes from the Σ pole diagram of the bare Jülich potential which moves 35 MeV up in energy due to the iteration process involved in T -matrix. Hence, the peak in the spectral function is the in-medium reflection of this singularity in the free space T -matrix. The dotted line shows the spectral density at $\rho = \rho_0$ but keeping only the $L = 0$ component of the $\bar{K}N$ interaction. In agreement with the behavior of the optical potential at zero momentum, we observe that the location of the quasiparticle peak only moves a few MeV, while the width (height) gets reduced (increased) by about 30%.

IV. CONCLUSIONS

We have performed a microscopic self-consistent calculation of the single-particle potential of a \bar{K} meson embedded in symmetric nuclear matter, using the meson-exchange Jülich $\bar{K}N$ interaction.

Due to the strong energy dependence of the $\bar{K}N$ G -matrix it becomes crucial to follow a self-consistent procedure to evaluate the \bar{K} self-energy. In this work we have analyzed two self-consistent schemes which produce substantial different results. When only the real part of the \bar{K} optical potential is retained in the self-consistent procedure, one obtains an attraction of about -100 MeV at zero momentum and a very small imaginary part of around -3 MeV. This optical potential would lead to extremely narrow deeply bound kaonic states in nuclei. However, when the complete complex optical potential is self-consistently determined, the real part becomes 15% less attractive and the imaginary part increases to around -25 MeV, as a consequence of the widening of the antikaon strength which produces a $\bar{K}N$ amplitude smoother and more spread out over energies.

We have obtained the kaon optical potential as a function of the \bar{K} momentum, up to regions that are relevant in the analysis of heavy-ion collisions where antikaons are created with a finite momentum. Our results for the optical potential show a momentum dependence

which is moderate for the real part and significantly more relevant for the imaginary part, which is especially important for densities around the saturation density.

We have also studied the effect of including the higher partial waves of the $\bar{K}N$ interaction. Some influence is already seen at zero \bar{K} momentum but the largest effects appear clearly at large momenta, where the inclusion of the $L > 0$ partial waves of the $\bar{K}N$ interaction can practically double the size of the optical potential. At a \bar{K} momentum of 500 MeV/c the complex optical potential changes from the $L = 0$ value of $(-28, -39)$ MeV to $(-52, -61)$ MeV when all partial waves are included.

ACKNOWLEDGMENTS

We are very grateful to Monika Hoffmann for providing us with the codes of the Jülich $\bar{K}N$ interaction and to E. Oset for useful discussions. This work is partially supported by DGICYT contract number PB98-1247 and by the Generalitat de Catalunya under project SGR98-11. One of us (L.T.) wishes to acknowledge support from a doctoral fellowship of the Ministerio de Educación y Cultura (Spain).

APPENDIX A

In this appendix we show how to compute the angular average of the Pauli operator, $Q_{\bar{K}N}$. Defining \vec{P} and \vec{k} as the total and relative momenta of the $\bar{K}N$ pair, respectively

$$\vec{P} = \vec{k}_{\bar{K}} + \vec{k}_N, \quad \vec{k} = \frac{M_N \vec{k}_{\bar{K}} - M_{\bar{K}} \vec{k}_N}{M_{\bar{K}} + M_N}, \quad (\text{A.1})$$

we can rewrite the nucleon and antikaon momenta in the laboratory system, \vec{k}_N and $\vec{k}_{\bar{K}}$, as

$$\vec{k}_N = -\vec{k} + \frac{\xi}{1+\xi} \vec{P}, \quad \vec{k}_{\bar{K}} = \vec{k} + \frac{1}{1+\xi} \vec{P}, \quad (\text{A.2})$$

where a galilean transformation has been used and $\xi = \frac{M_N}{M_{\bar{K}}}$. The Pauli operator acts only on the nucleonic line and, in symmetric nuclear matter, it reads

$$Q_{\bar{K}N}(\vec{P}, \vec{k}) = \theta \left(\left| \frac{\xi}{1+\xi} \vec{P} - \vec{k} \right| - k_F \right), \quad (\text{A.3})$$

which depends on the angle between \vec{P} and \vec{k} . In order to eliminate this dependence, we introduce an angle average

$$\bar{Q}_{\bar{K}N}(P, k) = \frac{1}{2} \int_0^\pi d\theta \sin \theta Q(\vec{P}, \vec{k}), \quad (\text{A.4})$$

such that the resulting function, given by

$$\bar{Q}_{\bar{K}N}(P, k) = \begin{cases} \frac{1}{2} \left[1 + \frac{k^2 + \left(\frac{\xi}{1+\xi} \right)^2 P^2 - k_F^2}{2kP \frac{\xi}{1+\xi}} \right] & \text{for } \left| \frac{\xi}{1+\xi} P - k_F \right| < k < \frac{\xi}{1+\xi} P + k_F, \\ 1 & \text{for } k > \frac{\xi}{1+\xi} P + k_F \text{ or } k < \frac{\xi}{1+\xi} P - k_F, \\ 0 & \text{otherwise} \end{cases}, \quad (\text{A.5})$$

depends only on the modulus of the relative and total momenta of the $\bar{K}N$ state.

APPENDIX B

In this appendix we show how to compute an appropriate average of the $\bar{K}N$ center-of-mass momentum, \vec{P} , and the nucleon momentum, \vec{k}_N , given an external antikaon momentum, $\vec{k}_{\bar{K}}$, and a relative $\bar{K}N$ momentum, \vec{k} , used as integration variable in Eq. (10). From Eqs. (A.1) and (A.2) one obtains

$$\vec{P} = (1 + \xi)(\vec{k}_{\bar{K}} - \vec{k}), \quad \vec{k}_N = \xi\vec{k}_{\bar{K}} - 1 + \xi\vec{k}. \quad (\text{B.1})$$

The angle average of the center-of-mass momentum is defined as

$$\overline{P^2}(k_{\bar{K}}, k) = \frac{\int d(\cos \theta) P^2(k_{\bar{K}}, k, \cos \theta)}{\int d(\cos \theta)}, \quad (\text{B.2})$$

where $P^2(k_{\bar{K}}, k, \cos \theta) = (1 + \xi)^2(k_{\bar{K}}^2 + k^2 - 2k_{\bar{K}}k \cos \theta)$, with θ being the angle between $\vec{k}_{\bar{K}}$ and \vec{k} . Similarly, for $\overline{k_N^2}$ we have

$$\overline{k_N^2}(k_{\bar{K}}, k) = \frac{\int d(\cos \theta) k_N^2(k_{\bar{K}}, k, \cos \theta)}{\int d(\cos \theta)}, \quad (\text{B.3})$$

where $k_N^2(k_{\bar{K}}, k, \cos \theta) = \xi^2 k_{\bar{K}}^2 + (1 + \xi)^2 k^2 - 2\xi(1 + \xi)k_{\bar{K}}k \cos \theta$.

In both cases, the integration runs from $\cos \theta_m$ to 1, where the expression for $\cos \theta_m$ depends on two regions of integration, according to the restrictions imposed by Pauli blocking, and is given by

$$\cos \theta_m = \begin{cases} \frac{\xi^2 k_{\bar{K}}^2 + (1 + \xi)^2 k^2 - k_F^2}{2\xi k_{\bar{K}}(1 + \xi)k} & \text{for } \frac{|k_F - \xi k_{\bar{K}}|}{1 + \xi} \leq k \leq \frac{k_F + \xi k_{\bar{K}}}{1 + \xi}, \\ -1 & \text{for } k \leq \frac{k_F - \xi k_{\bar{K}}}{1 + \xi} \end{cases} \quad (\text{B.4})$$

The resulting angle averages for \vec{P} and \vec{k}_N are given by

$$\overline{P^2}(k_{\bar{K}}, k) = \begin{cases} (1 + \xi)^2 \left[(k_{\bar{K}}^2 + k^2) - \frac{[\xi k_{\bar{K}} + (1 + \xi)k]^2 - k_F^2}{2\xi(1 + \xi)} \right] & \text{for } \frac{|k_F - \xi k_{\bar{K}}|}{1 + \xi} \leq k \leq \frac{k_F + \xi k_{\bar{K}}}{1 + \xi}, \\ (1 + \xi)^2 (k_{\bar{K}}^2 + k^2) & \text{for } k \leq \frac{k_F - \xi k_{\bar{K}}}{1 + \xi} \end{cases} \quad (\text{B.5})$$

$$\overline{k_N^2}(k_{\bar{K}}, k) = \begin{cases} \xi^2 k_{\bar{K}}^2 + (1 + \xi)^2 k^2 - \frac{[\xi k_{\bar{K}} + (1 + \xi)k]^2 - k_F^2}{2} & \text{for } \frac{|k_F - \xi k_{\bar{K}}|}{1 + \xi} \leq k \leq \frac{k_F + \xi k_{\bar{K}}}{1 + \xi}, \\ \xi^2 k_{\bar{K}}^2 + (1 + \xi)^2 k^2 & \text{for } k \leq \frac{k_F - \xi k_{\bar{K}}}{1 + \xi} \end{cases} \quad (\text{B.6})$$

REFERENCES

- [1] D.B. Kaplan and A.E. Nelson, Phys. Lett. B175 (1986) 57.
- [2] E. Friedman, A. Gal and C.J. Batty, Nucl. Phys. A579 (1994) 518.
- [3] S. Hirenzaki, Y. Okumura, H. Toki, E. Oset and A. Ramos, Phys. Rev. C61 (2000) 055205.
- [4] A. Ramos and E. Oset, Nucl. Phys. A671 (2000) 481.
- [5] E. Oset and A. Ramos, Nucl. Phys. A635 (1998) 99.
- [6] A. Baca, C. García-Recio and J. Nieves, Nucl. Phys. A, in print. nucl-th/0001060.
- [7] V. Koch, Phys. Lett. B337 (1994) 7.
- [8] T. Waas, N. Kaiser and W. Weise, Phys. Lett. B365 (1996) 12; *ibid.* B379 (1996) 34.
- [9] T. Waas and W. Weise, Nucl. Phys. A625 (1997) 287.
- [10] M. Lutz, Phys. Lett. B426 (1998) 12.
- [11] R. Barth et al., Phys. Rev. Lett. 78 (1997) 4007; F. Laue et al., Phys. Rev. Lett. 82 (1999) 1640.
- [12] W. Cassing, E.L. Bratkovskaya, U. Mosel, S. Teis and A. Sibirtsev, Nucl. Phys. A614 (1997) 415; E.L. Bratkovskaya, W. Cassing and U. Mosel, Nucl. Phys. A622 (1997) 593.
- [13] G.Q. Li, C.-H. Lee and G.Brown, Nucl. Phys. A625 (1997) 372; *ibid.*, Phys. Rev. Lett. 79 (1997) 5214.
- [14] G.Q. Li and G.Brown, Phys. Rev. C58 (1998) 1698.
- [15] A. Sibirtsev and W. Cassing, Nucl. Phys. A641 (1998) 476.
- [16] J. Schaffner-Bielich, V.Koch and M. Effenberg, Nucl. Phys. A669 (2000) 153.
- [17] A. Ohnishi, Y. Nara and V. Koch, Phys. Rev. C56 (1997) 2767.
- [18] H. Tamura et al. Phys Rev. C40 (1989) R479.
- [19] K. Kubota et al. Nucl. Phys. A602 (1996) 327.
- [20] A. Müller-Groeling, K. Holinde and J. Speth, Nucl. Phys. A513 (1990) 557.
- [21] R. Wiringa, Phys. Rev. C38 (1988) 2967.

FIGURES

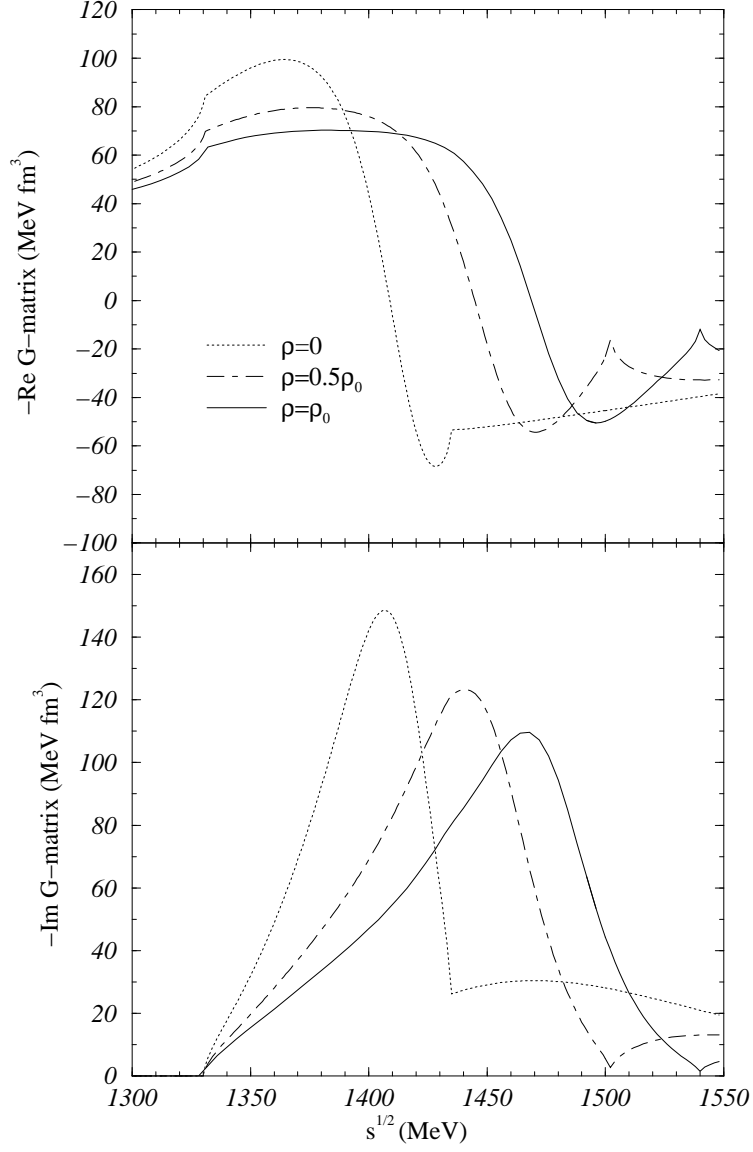


FIG. 1. Real and imaginary parts of the $\bar{K}N$ amplitude in the $I = 0, L = 0$ channel as functions of the center-of-mass energy at total momentum $|\vec{k}_{\bar{K}} + \vec{k}_N| = 0$ for various densities.

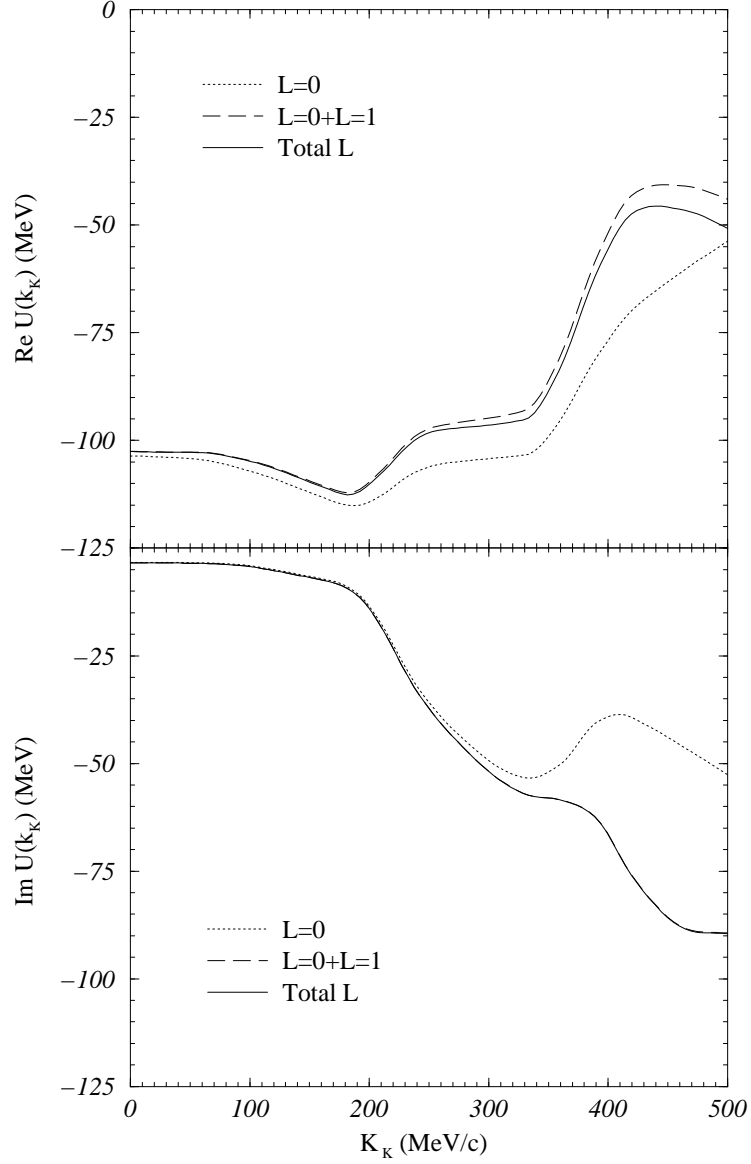


FIG. 2. Real and imaginary parts of the \bar{K} optical potential at $\rho = \rho_0$ as functions of the antikaon momentum. These results are obtained when only the real part of the \bar{K} potential is determined self-consistently.

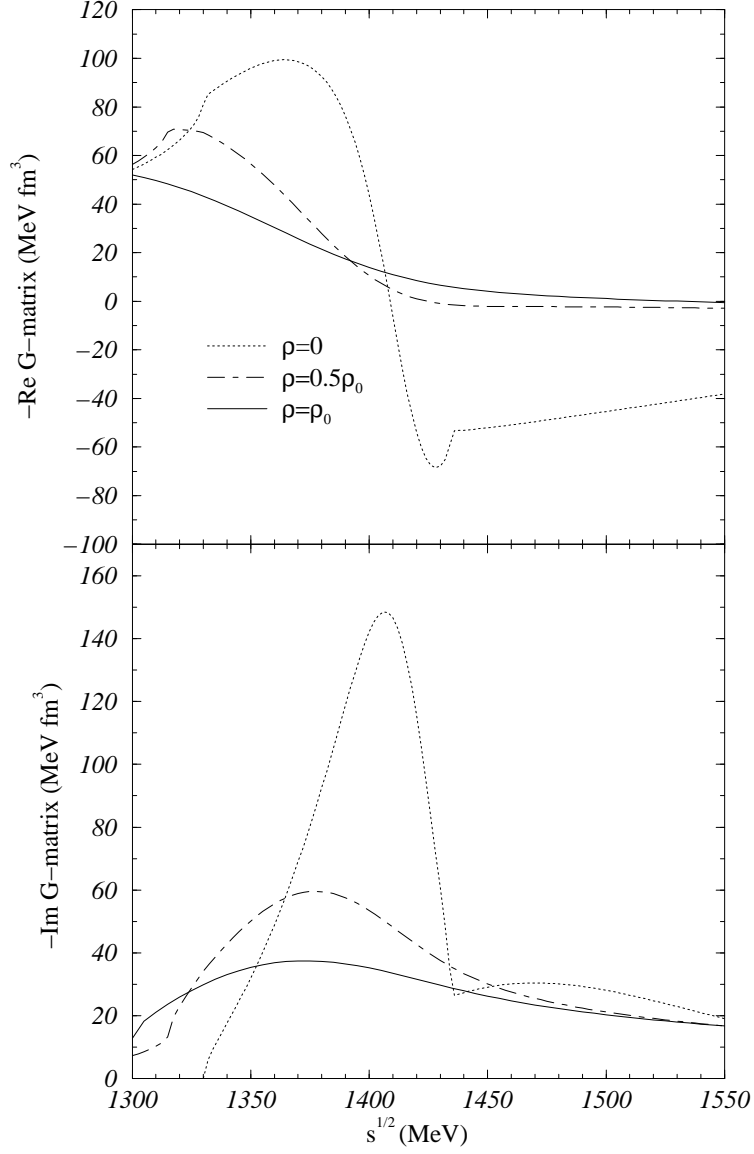


FIG. 3. Real and imaginary parts of the $\bar{K}N$ amplitude in the $I = 0, L = 0$ channel as functions of the center-of-mass energy at total momentum $|\vec{k}_{\bar{K}} + \vec{k}_N| = 0$ for various densities, as obtained from a self-consistent calculation with a complex \bar{K} optical potential.

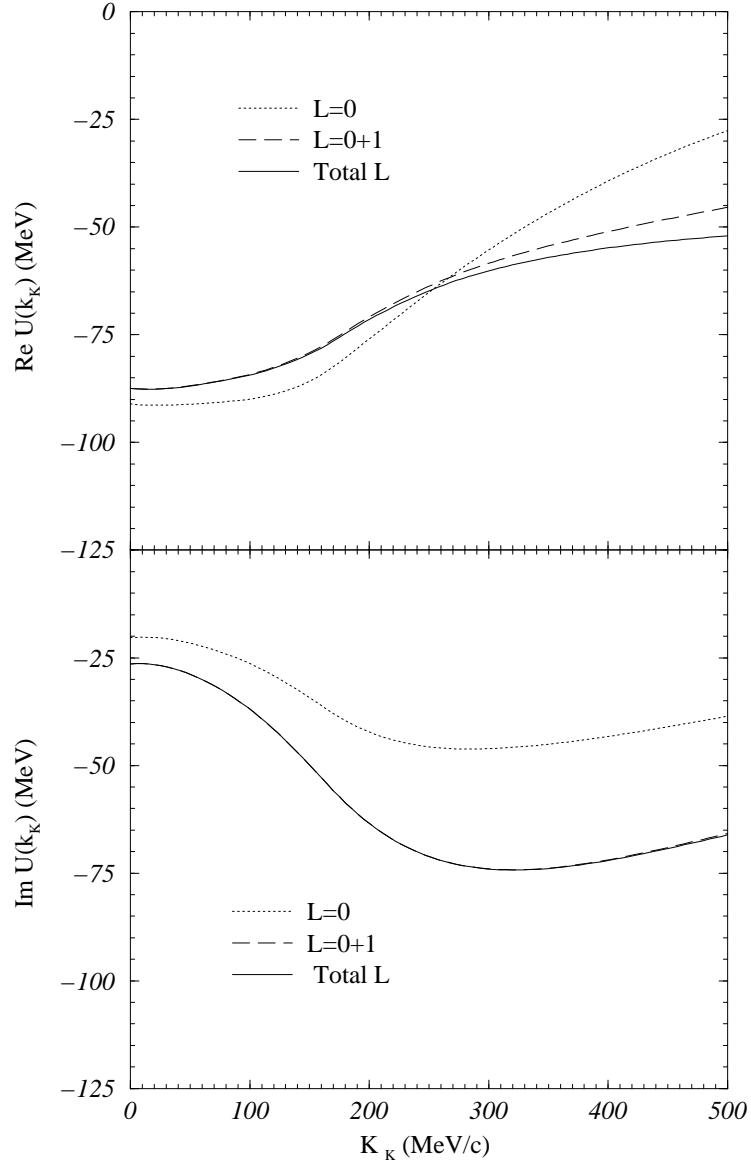


FIG. 4. Same as Fig. 2 but obtained from a self-consistent scheme which uses the complex \bar{K} optical potential.

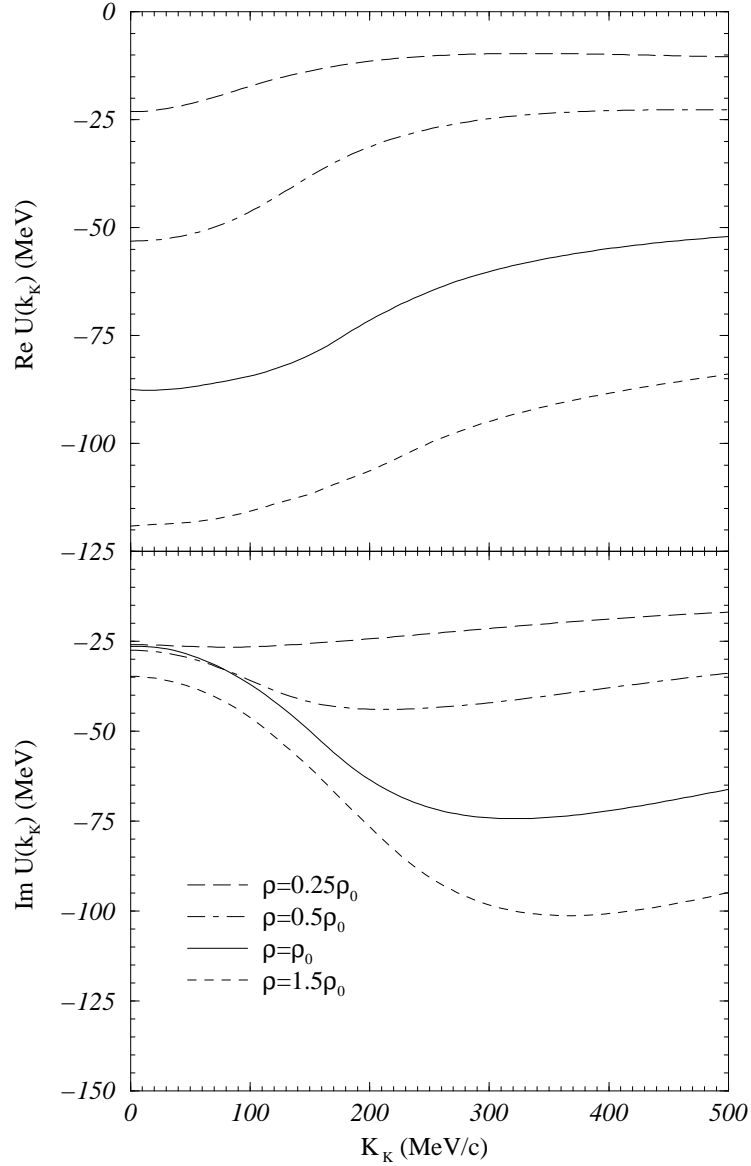


FIG. 5. Real and imaginary parts of the \bar{K} optical potential as functions of the antikaon momentum for various densities.

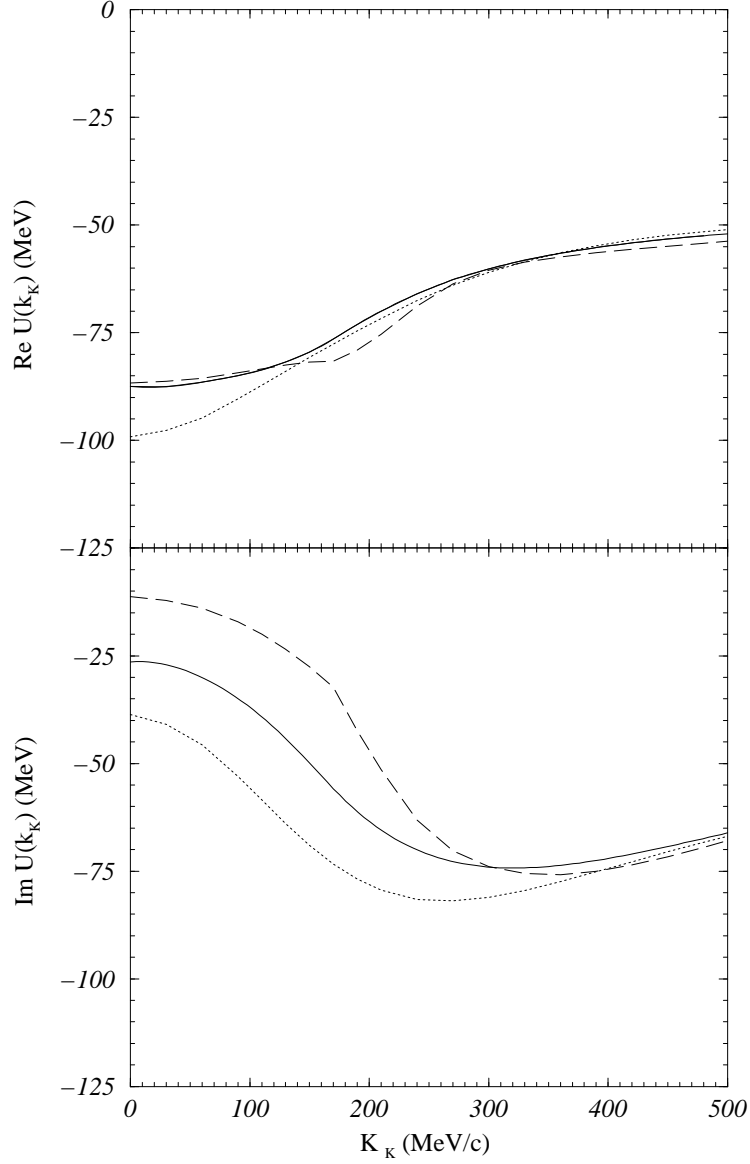


FIG. 6. Real and imaginary parts of the \bar{K} optical potential as functions of the antikaon momentum for various approximations. Solid line: our results. Dashed line: nucleon recoil corrections neglected. Dotted line: nucleon recoil corrections neglected and free-particle spectrum used for nucleons.

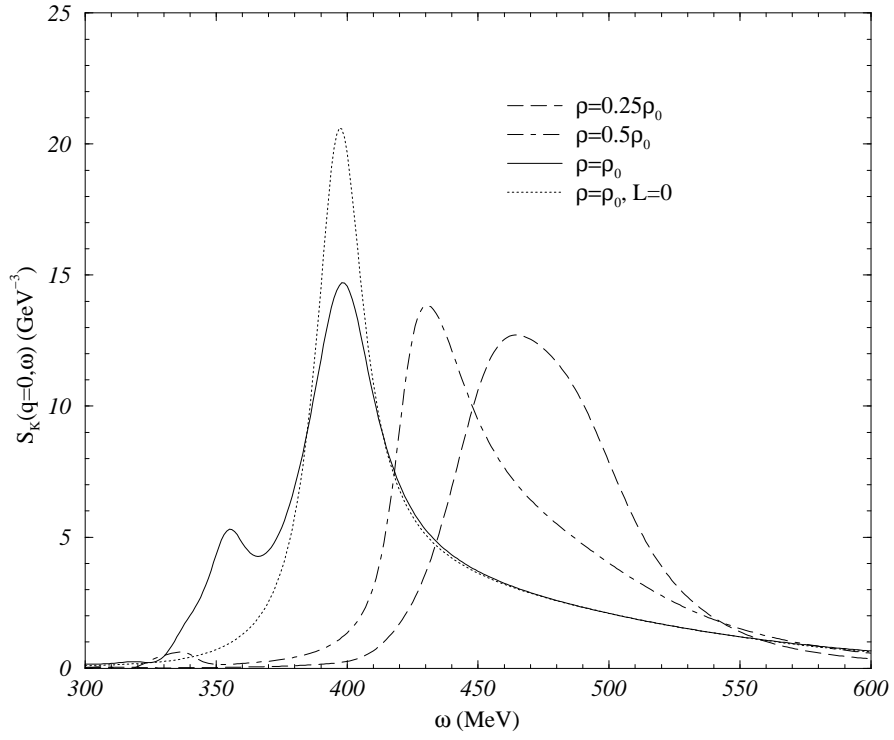


FIG. 7. \bar{K} spectral density at $k_{\bar{K}} = 0$ as a function of energy for various densities.